

Quantum impurity in a Tomonaga-Luttinger liquid: continuous-time quantum Monte Carlo approach

K. Hattori^{1,2*} and A. Rosch¹

¹*Institut für Theoretische Physik, Universität zu Köln, Zùlpicher Str., 77, D-50937 Köln, Germany*

²*Institute for Solid State Physics, University of Tokyo, 5-1-5, Kashiwanoha, Kashiwa, Chiba 277-8581, Japan*

(Dated: April 4, 2018)

We develop a continuous-time quantum Monte Carlo (CTQMC) method for quantum impurities coupled to interacting quantum wires described by a Tomonaga-Luttinger liquid. The method is negative-sign free for any values of the Tomonaga-Luttinger parameter, which is rigorously proved, and thus, efficient low-temperature calculations are possible. Duality between electrons and bosons in one dimensional systems allows us to construct a simple formula for the CTQMC algorithm in these systems. We show that the CTQMC for Tomonaga-Luttinger liquids can be implemented with only minor modifications of previous CTQMC codes developed for impurities coupled to non-interacting fermions. We apply this method to the Kane-Fisher model of a potential scatterer in a spin-less quantum wire and to a single spin coupled with the edge state of a two-dimensional topological insulator assuming an anisotropic XXZ coupling. Various dynamical response functions such as the electron Green's function and spin-spin correlation functions are calculated numerically and their scaling properties are discussed.

PACS numbers: 68.65.La, 71.10.Pm, 75.40.Mg

I. INTRODUCTION

Electronic correlations play fundamental roles in determining low-energy phenomena in one-dimensional electron systems [1, 2]. Bosonization is a powerful technique to treat such correlations exactly. In the presence of impurities, however, it is well known that impurities in one-dimensional systems drastically influence transport properties of the systems. Such an example has been found in a classical model by Kane and Fisher in their pioneering work about a backward scattering potential problem in a spinless quantum wire [3]. There, for the case of repulsive interaction [Tomonaga-Luttinger (TL) parameter $g < 1$], the conductance G vanishes at zero temperature ($T = 0$) and the potential barrier becomes infinitely strong and cut the wire into two parts, while for attractive cases with $g > 1$, the potential becomes zero in the low-energy limit and there remains a finite value of the conductance at $T = 0$.

For acquiring knowledge about thermodynamic, transport, and dynamical properties of such systems, bosonization combined with perturbative renormalization group methods [3–5], Bethe ansatz [6], and functional renormalization group [7] have been intensively used so far. To obtain numerically exact results for bosonized impurity problems, path integral Monte Carlo approaches have been employed [8–10]. A bosonic numerical renormalization group method [11] is also a powerful technique to investigate their low-energy properties. While they are very useful approaches, there is still need for even more powerful numerical approaches that allow to compute wide range of temperature properties and

dynamical correlation functions even for more complex models in an exact way.

To this end, in this paper, we will develop a continuous-time quantum Monte Carlo (CTQMC) method [12–15] in the Tomonaga-Luttinger liquid (TLL) in one-dimensional systems coupled to an impurity. The CTQMC previously has been developed to describe quantum impurities coupled to *non-interacting* environments. It has mainly been used for fermionic systems and extensively used in the frame work of the dynamical mean field theory [16] as an exact numerical solver for the effective-impurity problem in it. Recent development [17, 18] of the algorithm also enables us to treat bosonic systems and mixture of bosons and fermions. The advantage of the CTQMC is that this allows us to calculate various quantities at low temperatures in efficient ways and for some simple models there is no negative sign problem [13, 14].

Our algorithm of CTQMC for TLL has advantages in the following points. (i) Bosonization allows us to treat correlation arising from strong interactions in the environment exactly. (ii) There is no negative sign problem for any parameters, which is, indeed, proved analytically. This enables us to carry out low-temperature analysis with high precision. (iii) There are close relations to the fermionic version of CTQMC, although the whole algorithm is written in the bosonization language. This enables ones to implement the CTQMC for the TLL easily from their fermionic CTQMC code. (iv) The method can be applicable to not only potential scattering problems but also to Kondo-type problems [19–21] without a negative sign problem. (v) The electron Green's functions, the boson-boson correlations, conductance, the spin-spin correlation functions, and various local correlators are calculable. (vi) Compared with lattice QMCs, our formalism is free from finite size effects at low temperatures

* hattori@issp.u-tokyo.ac.jp

and phase spaces for the random walk is expected to be much smaller, and, thus, the computational cost is much lower.

This paper is organized as follows. In Sec. II, we will explain the models used in this paper. Section III will be devoted to illustrate our algorithm of the CTQMC for TLL. The method will be applied to the Kane-Fisher model [3] in Sec. IV A and the XXZ Kondo problem [19–21] in Sec. IV B. We will discuss possible extension in Sec. V and summarize the present results in Sec. VI.

II. MODELS

In this section, we will introduce our model. First, we will show a one-dimensional Tomonaga-Luttinger liquid Hamiltonian and explain our notation of the bosonization we will use throughout this paper. The second part is an introduction of impurity-electron interactions. We will use a general expression that can be used in two models we will discuss in Sec. IV.

A. One-dimensional bulk Hamiltonian

We consider spin-less fermions in one-dimensional (1D) systems whose non-interacting Hamiltonian is given by [2]

$$H_{1D} = \frac{iv_F}{2\pi} \int_{-\frac{l}{2}}^{\frac{l}{2}} dx : \left\{ \psi_L^\dagger(x) \partial_x \psi_L(x) - \psi_R^\dagger(x) \partial_x \psi_R(x) \right\} :, \quad (1)$$

where $\psi_{L,R}^\dagger(x)$ is the fermion creation operator at the position x and $L(R)$ refer to left(right)-moving component. $:A:$ indicates the normal ordering of the operator A , l is the system size, and v_F is the Fermi velocity. The fermion field $\psi_{L,R}(x)$ satisfies the anticommutation relation

$$\{\psi_\rho(x), \psi_{\rho'}^\dagger(x')\} = 2\pi \delta_{\rho\rho'} \delta(x - x'). \quad (2)$$

Following the standard bosonization procedure [2, 4], we define bosons $\phi_{L,R}(x)$ as

$$\psi_{L,R}(x) = a^{-1/2} F_{L,R} e^{i\phi_{L,R}(x)}, \quad (3)$$

where a is the short-distance cutoff. The Bose fields satisfy

$$[\phi_\rho(x), \partial_{x'} \phi_{\rho'}(x')] = 2\pi i \delta_{\rho\rho'} \left[\delta(x - x') - \frac{1}{2l} \right], \quad (4)$$

where the $O(l^{-1})$ term is explicitly written. Two Klein factors F_L and F_R have been introduced in Eq. (3) to reproduce the anticommutation relation of $\psi_{R,L}$ [Eq. (2)]. Their anticommutation relation is

$$\{F_\rho, F_{\rho'}^\dagger\} = 2\delta_{\rho\rho'} \quad \text{with} \quad F_\rho^\dagger F_\rho = F_\rho F_\rho^\dagger = 1, \quad (5)$$

and

$$\{F_\rho^\dagger, F_{\rho'}^\dagger\} = \{F_\rho, F_{\rho'}\} = 0, \quad \text{for } \rho \neq \rho'. \quad (6)$$

Note that $F_\rho F_\rho \neq 1$, and the two bosons are independent fields commuting with each other and with the Klein factors, which is a physically correct description as is evident from the definition of L and R [4].

Electron-electron interactions are easily taken into account in the bosonized theory and then the bosonized Hamiltonian reads

$$H_{1D} = \frac{v}{4} \int_{-\frac{l}{2}}^{\frac{l}{2}} \frac{dx}{2\pi} : \left\{ \frac{1}{g} \left[\partial_x \phi_-(x) \right]^2 + g \left[\partial_x \phi_+(x) \right]^2 \right\} :, \quad (7)$$

with $\phi_\pm(x) = \phi_L(x) \pm \phi_R(x)$ and g is the TL parameter that characterizes the bosonic theory: $g = 1$ corresponds to the noninteracting case and $0 < g < 1$ ($g > 1$) describes repulsive (attractive) interactions, respectively. The velocity v_F is now renormalized as $v \equiv v_F/g$. Throughout this paper, we will be interested in the repulsive case.

For later purposes, we introduce another representation following Delft and Schoeller as [4]

$$\Phi_\pm(x) = \frac{1}{2\sqrt{2}} \left\{ \left(\frac{1}{\sqrt{g}} + \sqrt{g} \right) \left[\phi_L(x) \mp \phi_R(-x) \right] \pm \left(\frac{1}{\sqrt{g}} - \sqrt{g} \right) \left[\phi_L(-x) \mp \phi_R(x) \right] \right\}. \quad (8)$$

Then, the Hamiltonian (7) is rewritten as

$$H_{1D} = \frac{v}{2} \int_{-\frac{l}{2}}^{\frac{l}{2}} \frac{dx}{2\pi} : \left\{ \left[\partial_x \Phi_-(x) \right]^2 + \left[\partial_x \Phi_+(x) \right]^2 \right\} :, \quad (9)$$

At $x = 0$, a simple relation holds [4],

$$\Phi_\pm \equiv \Phi_\pm(0) = \frac{g^{\mp 1/2}}{\sqrt{2}} \left[\phi_L(0) \mp \phi_R(0) \right]. \quad (10)$$

B. Impurity potentials

Now, we introduce interactions between a quantum impurity located at $x = 0$ and the interacting electrons of the TLL. We consider a coupling by single-particle scattering (generalization to more complicated interactions is straightforward but, of course, model dependent). The interactions, $V = V_F^\sigma + V_B$, are decomposed into two parts, a forward-scattering channel, V_F^σ , and a backward-scattering channel described by V_B ,

$$V_F^\sigma = \lambda_F : \left[\psi_L^\dagger(0) \psi_L(0) - \sigma \psi_R^\dagger(0) \psi_R(0) \right] : \hat{X}_F^\sigma, \quad (11)$$

$$V_B = \lambda_B \psi_L^\dagger(0) \psi_R(0) \hat{X}_B + \text{H.c.}, \quad (12)$$

The scattering of electrons can change the state of the impurity (e.g., flip a spin). This is described by the impurity operators $\hat{X}_F^{\sigma=\pm}$ and \hat{X}_B . They will be discussed in later sections. In the most general case, their form can be derived by first bosonizing the model and then identifying the two terms discussed above by comparing them to the bosonized version of Eqs. (11) and (12)

discussed below. Note that $\lambda_{F,B}$ has the dimension of [energy]×[length] and \hat{X} 's are dimensionless operators.

In terms of the bosons, Eqs. (11) and (12) read

$$V_F^\sigma = \lambda_F \sqrt{\frac{2}{g^\sigma}} \partial_x \Phi_\sigma(0) \hat{X}_F^\sigma, \quad (13)$$

$$\begin{aligned} V_B &= a^{g-1} \lambda_B F_L^\dagger F_R \left(a^{-g} e^{i\sqrt{2g}\Phi_+} \right) \hat{X}_B \\ &\quad + a^{g-1} \lambda_B^* F_R^\dagger F_L \left(a^{-g} e^{-i\sqrt{2g}\Phi_+} \right) \hat{X}_B^\dagger \\ &\equiv \tilde{\lambda}_B F_L^\dagger F_R \hat{V}_{+\sqrt{2g}}(\Phi_+) \hat{X}_B^+ + \tilde{\lambda}_B^* F_R^\dagger F_L \hat{V}_{-\sqrt{2g}}(\Phi_+) \hat{X}_B^-, \end{aligned} \quad (14)$$

where $\hat{X}_B^+ = \hat{X}_B$, $\hat{X}_B^- = \hat{X}_B^\dagger$, and $\tilde{\lambda}_B = a^{g-1} \lambda_B$. The vertex operator is defined as

$$V_{\pm\sqrt{2g}}(\Phi_+) = a^{-g} \exp\left(\pm i\sqrt{2g}\Phi_+\right). \quad (16)$$

This normalization of the vertex operator leads to following the bare (i.e., in the absence of the impurity) two-point correlator as a function of imaginary time τ ,

$$\langle V_{\sqrt{2g}}(\Phi_+, \tau) V_{-\sqrt{2g}}(\Phi_+, \tau') \rangle = |\tau - \tau'|^{-2g}, \quad (17)$$

at $T \rightarrow 0$ for $a \rightarrow 0$ and $l \rightarrow \infty$ [see also the definition of multipoint correlators in Eq. (28) below].

III. CONTINUOUS-TIME QUANTUM MONTE CARLO METHOD

In this section, we will explain how continuous-time quantum Monte Carlo method can be applied to the impurity problem in the TLLs. We will demonstrate that the configuration weight for a given snapshot is easily calculated by the technique developed in fermionic CTQMCs. We will therefore omit detailed explanations about update operations, since these are essentially the same as in the fermionic CTQMCs [15].

A. Partition function

We want to evaluate the partition function Z ,

$$Z = \text{Tr} \exp[-\beta(H_0 + V)], \quad (18)$$

within a Monte Carlo approach. Here, the ‘‘noninteracting’’ part H_0 is the sum of the one-dimensional TLL and the local impurity Hamiltonian, $H_0 = H_{1D} + H_{\text{imp}}$. In this paper, we will analyze models with $H_{\text{imp}} = 0$ (e.g., a magnetic impurity in the absence of magnetic fields). Via perturbative expansion of V , we can express Z as

$$\frac{Z}{Z_0} = \left\langle T_\tau \exp \left[- \int_0^\beta V(\tau) d\tau \right] \right\rangle_0, \quad (19)$$

where $Z_0 = \text{Tr} e^{-\beta H_0}$ and $\langle A \rangle_0 = [\text{Tr} A e^{-\beta H_0}] / Z_0$ and T_τ indicates the time-ordered product. In this paper, we will

discuss situations where the forward-scattering part (λ_F) can be eliminated by an appropriate unitary transformation or where $\lambda_F = 0$ due to symmetry requirements. Thus, we retain only V_B and in order to distinguish the two terms in V_B , we define

$$v_B^+ \equiv \tilde{\lambda}_B F_L^\dagger F_R \hat{V}_{+\sqrt{2g}}(\Phi_+) \hat{X}_B^+, \quad (20)$$

$$v_B^- \equiv \tilde{\lambda}_B^* F_R^\dagger F_L \hat{V}_{-\sqrt{2g}}(\Phi_+) \hat{X}_B^-. \quad (21)$$

A general N th order term δZ_N in the partition function is expressed as

$$\begin{aligned} \delta Z_N &= \frac{(-1)^N}{N!} \int_0^\beta d\tau_1 \cdots \int_0^\beta d\tau_N \\ &\quad \times \langle T_\tau V_B(\tau_1) V_B(\tau_2) \cdots V_B(\tau_N) \rangle_0. \end{aligned} \quad (22)$$

Due to the fermion number conservation encoded by the Klein factors, the number of v_B^+ in Eq. (22) has to be the same as that for v_B^- , and therefore only even $N = 2k$ terms with $k \in \mathbb{Z}$, contribute. Now, consider a fixed series of times $\{\tau; \tau_1 > \tau_2 > \cdots > \tau_N\}$. Then $\delta Z_N\{\tau\}$ becomes

$$\delta Z_N\{\tau\} = |\tilde{\lambda}_B|^{2k} \langle v_B^{\sigma_1}(\tau_1) v_B^{\sigma_2}(\tau_2) \cdots v_B^{\sigma_{2k}}(\tau_{2k}) \rangle_0, \quad (23)$$

with $\sigma_1, \sigma_2, \cdots, \sigma_{2k} = +$ or $-$. The partition sum is obtained by averaging over all σ_i , all times, and all k using a Monte Carlo procedure.

Since the product of Klein factors gives factor unity, we can write Eq. (23) as a product of a TLL correlator and a correlator involving only impurity operators

$$\delta Z_{2k}\{\tau\} = |\tilde{\lambda}_B|^{2k} \delta Z_{2k}^{\Phi_+}\{\tau\} \delta Z_{2k}^X\{\tau\}. \quad (24)$$

In the following subsections, we will analyze the two sectors in details.

B. Impurity average

Here, we discuss the local part δZ_{2k}^X . δZ_{2k}^X is the time-ordered product of \hat{X}_B^\pm 's:

$$\delta Z_{2k}^X\{\tau\} = \langle \hat{X}_B^{\sigma_1}(\tau_1) \cdots \hat{X}_B^{\sigma_{2k}}(\tau_{2k}) \rangle_{\text{imp}}. \quad (25)$$

Here, $\langle \cdot \rangle_{\text{imp}}$ is the average with respect to the impurity Hamiltonian. As noted above, both \hat{X}_B^+ and \hat{X}_B^- appear k times and, for later convenience, we define new τ indices τ_i^\pm with $1 \leq i \leq k$, such that the operators \hat{X}_B^+ (\hat{X}_B^-) are evaluated at the times τ_i^+ (τ_i^-) with time-ordering in each index, $\tau_i^\pm > \tau_{i+1}^\pm$.

C. Boson average

For the bosonic part, $\delta Z_{2k}^{\Phi_+}$ is the time-ordered $2k$ -point correlation function of $\hat{V}_{\pm\sqrt{2g}}(\Phi_+)$:

$$\delta Z_{2k}^{\Phi_+}\{\tau\} = \langle \hat{V}_{\sigma_1\sqrt{2g}}(\Phi_+, \tau_1^{\sigma_1}) \cdots \hat{V}_{\sigma_{2k}\sqrt{2g}}(\Phi_+, \tau_{2k}^{\sigma_{2k}}) \rangle_{\Phi_+}. \quad (26)$$

Here, the boson average $\langle \cdot \rangle_{\Phi_+}$ is evaluated using the Gaussian TLL Hamiltonian (9). It is well known that the correlation function of vertex operators,

$$\hat{V}_{\lambda_i}(\Phi_+, \tau_i) = a^{-\lambda_i^2/2} e^{i\lambda_i \Phi_+(\tau_i)}, \quad (27)$$

are calculated as [4]

$$\begin{aligned} & \langle T_\tau \hat{V}_{\lambda_1}(\Phi_+, \tau_1) \cdots \hat{V}_{\lambda_N}(\Phi_+, \tau_N) \rangle_{\Phi_+} \\ &= \left(\frac{2\pi}{l} \right)^{\frac{1}{2}} \left(\sum_j \lambda_j \right)^2 \prod_{i < j} [s(\tau_{ij})]^{\lambda_i \lambda_j}, \end{aligned} \quad (28)$$

with

$$s(\tau_{ij}) \equiv \frac{v\beta}{\pi} \sin \left[\frac{\pi}{v\beta} (v|\tau_{ij}| + \epsilon(|\tau_{ij}|)) \right]. \quad (29)$$

Here, $\tau_{ij} = \tau_i - \tau_j$, and, in order to prevent the divergence, the cutoff function $\epsilon(\tau)$ is necessary and it satisfies

$$\epsilon(\tau) = -\epsilon(\beta - \tau), \quad \epsilon(0) = a, \quad \text{and} \quad \epsilon(\beta) = -a. \quad (30)$$

In actual calculations, we will use the following function $\epsilon(\tau)$ throughout this paper:

$$\epsilon(\tau) = a \operatorname{sgn}(\beta/2 - \tau). \quad (31)$$

For very high temperatures (not considered in this paper), it is sometimes useful to use a smooth function in order to remove the discontinuity appearing in physical quantities such as

$$\epsilon(\tau) = a \tanh \left[c \frac{\beta/2 - \tau}{\tau(\beta - \tau)} \right], \quad (32)$$

with c being a positive constant. In the $l \rightarrow \infty$ limit, Eq. (28) vanishes unless $\sum_j \lambda_j = 0$. Thus, a ‘‘neutrality condition,’’ $\sum_j \lambda_j = 0$, has to be fulfilled. In our case, this is automatically enforced by the fermion number conservation and we obtain

$$\delta Z_{2k}^{\Phi_+} \{\tau\} = \prod_{i < j} [s(\tau_{ij})]^{\lambda_i \lambda_j} > 0, \quad (33)$$

with $\lambda_{i,j} = \pm\sqrt{2g}$. An important observation is that Eq. (33) is positive definite, and, thus, our Monte Carlo method is negative-sign free if $\delta Z_{2k}^X > 0$.

Equation (33) can be further simplified via the ‘‘generalized’’ Wick’s theorem [4], which is valid if and only if $a = 0$. We utilize this theorem, although actual numerical calculations are done with finite a . The theorem might be most easily obtained by comparing the partition function for noninteracting spinless fermion in one dimension and that in the bosonization representation. The result is

$$\delta Z_{2k}^{\Phi_+} \{\tau\} = |\det \hat{S}_k \{\tau\}|^{2g}. \quad (34)$$

The $k \times k$ matrix \hat{S}_k is given by

$$[\hat{S}_k \{\tau\}]_{ij} = -\operatorname{sgn}(\tau_{ij}) [s(\tau_{ij})]^{-1}, \quad 1 \leq i, j \leq k, \quad (35)$$

and the index $i(j)$ corresponds to $\tau_i^-(\tau_j^+)$. This form is particularly useful, since we can use the fast-update algorithm developed in the conventional fermionic CTQMC methods [12].

IV. APPLICATIONS

In this section, we will apply our CTQMC method to two models. One is the Kane-Fisher model describing a backward-scattering impurity potential in a (spinless) quantum wire [3]. The other is the XXZ Kondo problem [19–21] in helical liquids, i.e., on the edge of two-dimensional topological insulators.

A. Kane-Fisher model

The Kane-Fisher model is defined by considering forward scattering \hat{X}_F^σ with $\sigma = -$ and $\hat{X}_F^- = 1$ in Eq. (11) and by setting $\hat{X}_B = \hat{X}_B^\dagger = 1$ in Eq. (12) as a potential scatterer has no internal degrees of freedom. Since V_F contains only Φ_- and V_B only Φ_+ , we can separately analyze the two. The V_F part is trivial because it can be absorbed into Φ_- terms in H_{1D} by a unitary transformation [4]. Thus, in the following, we analyze V_B part in details. Note that because $\hat{X}_B = 1$ and thus $\delta Z_{2k}^X = 1$, we can use the positivity of (33) to conclude immediately that there is no negative-sign problem. Throughout this subsection, we set $v = v_F/g$ and fix $v_F/\xi = 1$ for the unit of energy, where $\xi = 1$ is the relevant microscopic unit of length, which is, for example, set by the typical width of the potential.

The model itself has been extensively analyzed by various authors [3–9], and now its low-energy properties are well understood. We will study this problem as a benchmark of our algorithm. We will discuss a physical quantity that has not been investigated so far: the electron Green’s function in imaginary time. This is the most natural quantity for imaginary-time algorithms like CTQMC. Though it is not a directly measurable quantity in experiments, the numerically-exact results can be used to obtain the density of states by using analytical continuation techniques [22] (not covered in this paper).

1. Electron Green’s function

Let us consider the local Green’s function for $\psi_L(\tau > 0, x = 0)$,

$$\begin{aligned} G_L(\tau) &= -\langle \psi_L(\tau) \psi_L^\dagger(0) \rangle \\ &= -a^{\frac{g}{2} + \frac{1}{2g} - 1} \langle \hat{V}_{-\frac{1}{\sqrt{2g}}}(\Phi_-, \tau) \hat{V}_{\frac{1}{\sqrt{2g}}}(\Phi_-, 0) \rangle_{\Phi_-} \\ &\quad \times \langle F_L(\tau) F_L^\dagger(0) \rangle_F \langle \hat{V}_{-\sqrt{\frac{g}{2}}}(\Phi_+, \tau) \hat{V}_{\sqrt{\frac{g}{2}}}(\Phi_+, 0) \rangle_{\Phi_+} \\ &\equiv -a^{\frac{g}{2} + \frac{1}{2g} - 1} G_L^-(\tau) G_L^+(\tau), \end{aligned} \quad (36)$$

with

$$G_L^-(\tau) = \langle \hat{V}_{-\frac{1}{\sqrt{2g}}}(\Phi_-, \tau) \hat{V}_{\frac{1}{\sqrt{2g}}}(\Phi_-, 0) \rangle_{\Phi_-}, \quad (38)$$

$$G_L^+(\tau) = \langle F_L(\tau) F_L^\dagger(0) \rangle_F \langle \hat{V}_{-\sqrt{\frac{g}{2}}}(\Phi_+, \tau) \hat{V}_{\sqrt{\frac{g}{2}}}(\Phi_+, 0) \rangle_{\Phi_+}. \quad (39)$$

Here, $\langle \dots \rangle_F$ is the average over Klein factors. The correlation function for the Φ_- part $G_L^-(\tau)$ is trivial, leading to

$$G_L^-(\tau) = [s(\tau)]^{-\frac{1}{2g}}. \quad (40)$$

Here $s(\tau)$ is given by Eq. (29). Note that for our model nonlocal Green's function can be expressed in terms of local correlators as the bosons of the TLL are noninteracting. In the following, we explain how one can calculate the Φ_+ and the Klein factor parts $G_L^+(\tau)$ in our CTQMC.

In the Monte Carlo simulations, time-ordered averages of an operator \hat{A} is estimated as

$$\langle T_\tau \hat{A} \rangle = \frac{1}{N_{\text{MC}}} \sum_{m=1}^{N_{\text{MC}}} \frac{\langle T_\tau \hat{A} \delta \hat{Z}_{N_m} \{\tau\} \rangle_0}{\delta Z_{N_m} \{\tau\}}, \quad (41)$$

where N_{MC} is the number of Monte Carlo samplings and we have defined an operator form of $\delta Z_{N_m} \{\tau\}$, see Eq. (23). For $N_m = 2k$, this is given by

$$\delta \hat{Z}_{2k} \{\tau\} = |\tilde{\lambda}_B|^{2k} v_B^{\sigma_1}(\tau_1) v_B^{\sigma_2}(\tau_2) \cdots v_B^{\sigma_{2k}}(\tau_{2k}). \quad (42)$$

For the Green's function $G_L^+(\tau_{ij})$, we need to calculate Eq. (41) with $\hat{A} = F_L(\tau_i) \hat{V}_{-\eta}(\Phi_+, \tau_i) F_L^\dagger(\tau_j) \hat{V}_\eta(\Phi_+, \tau_j)$ with $\eta = \sqrt{g/2}$. As derived in Appendix A, we need to sample the following quantity for $\tau_{ij} > 0$,

$$\mathcal{G}_{i>j}^{(2k)} = (-1)^{P_{ij}} [s(\tau_{ij})]^{\frac{g}{2}} \left| \frac{\det \hat{S}_{k+1} \{\tau \oplus \tau_i, \tau_j\}}{\det \hat{S}_k \{\tau\}} \right|^g. \quad (43)$$

Here, P_{ij} is the number of vertices between τ_i and τ_j in the MC snapshot and a similar expression is obtained for $\tau_{ij} < 0$. The notation $\{\tau \oplus \tau_i, \tau_j\}$ represents that τ_i and τ_j are added to $\{\tau\}$. Note that to derive Eq. (43), we have used the generalized Wick's theorem mentioned before. Then we obtain

$$G_L^+(\tau_{ij}) = \langle \mathcal{G}_{i>j}^{(2k)} \rangle, \quad \text{for } \tau_{ij} > 0, \quad (44)$$

and a similar expression is applied to $G_L^+(\tau_{ij} < 0) = -G_L^+(\beta + \tau_{ij})$.

An alternative approach is, however, more efficient in regimes where high orders of perturbation theory are needed. Following Refs. [12, 13], we can also derive an alternative expression for calculating the Green's function $G_L^+(\tau)$. The quantity that corresponds to Eq. (43) is now given by

$$\tilde{\mathcal{G}}_{i>j}^{(2k)} = \frac{(-1)^{P_{ij}}}{|\tilde{\lambda}_B|^2} [s(\tau_{ij})]^{\frac{g}{2}} \left| \frac{\det \hat{S}_{k-1} \{\tau \ominus \tau_i^-, \tau_j^+\}}{\det \hat{S}_k \{\tau\}} \right|^g. \quad (45)$$

Note that in Eq. (45), τ_i^- and τ_j^+ are chosen in a given snapshot $\{\tau\}$, while in Eq. (43), τ_i and τ_j are external ones. This implies that by computing one snapshot with k pairs of time variables one obtains contribution to the Green's function for about k^2 different τ_{ij} , which helps to reduce the statistical error. The notation $\{\tau \ominus \tau_i, \tau_j\}$ represents that τ_i and τ_j are removed from $\{\tau\}$.

Since the ratio of two determinants in Eq. (45) is simply $(\hat{S}_k^{-1} \{\tau\})_{ji}$, which is calculated in every MC process, this also reduces computational costs [12, 13]. We can also derive a similar expression for $\tau_i < \tau_j$, $\tilde{\mathcal{G}}_{i<j}^{(2k)}$. Summing over all possible combinations (i, j) for a given snapshot at $2k$ th order and dividing by β , we obtain

$$G_L^+(\tau) = \frac{1}{\beta} \left\langle \sum_{ij}^k \left[\tilde{\mathcal{G}}_{i>j}^{(2k)} \delta(\tau_{ij} - \tau) - \tilde{\mathcal{G}}_{i<j}^{(2k)} \delta(\beta + \tau_{ij} - \tau) \right] \right\rangle. \quad (46)$$

The two alternative formulas (44) and (46) can be used for checking the program code.

2. Bench mark for $g = 1$

In this subsection, we show the results for $g = 1$, i.e., a system of noninteracting electrons. We compare the electron Green's function obtained in the CTQMC and the exact results as follows:

$$G_L^{+, \text{ex}}(\tau) = \frac{[s(\tau)]^{-\frac{1}{2}}}{1 + \pi^2 \lambda_B^2 / v^2}, \quad (47)$$

which can be easily obtained from the equations of motion for the Green's functions.

Figure 1 shows $G_L^+(\tau)$ as a function of τ for $\beta = 200$ and several parameters λ and a . In each plot, the exact result (dashed lines) and the result of the two methods described above are shown. The points with error bars (indicating the statistical error arising from the Monte Carlo sampling) are obtained from Eq. (43), while the solid lines have been calculated from Eq. (45) (the statistical error can be read off from the size of the noise in the curves). As one can see, the numerical data and the exact results are consistent with each other. More precisely, the Green's functions are only identical in the limit $a \rightarrow 0$ [we used this limit both in the derivation of the CTQMC approach and in Eq. (47)]. Figure 1 shows that tiny systematic deviations of the exact and the numerical result visible for $a = 1$ become smaller than the noise for $a = 0.25$. In the following, we will always use $a = 1$ as the universal properties for $T \ll v/a$ and $\tau \gg a/v$ discussed in the following are independent of the cutoff.

Figure 1 shows that highly accurate results are also obtained for low T . Comparing the two computational methods (using the same computational time), we first note that both give reliable results. Which method is preferable depends in general both on the perturbation order and the type of binning in time used to extract data. For the parameter regime used in our calculations, we found the second approach to be more efficient. For very high orders of perturbation theory and small number of bins, however, the first approach can beat the second one in efficiency. In Sec. V A, we will discuss that in regimes, where the nonlinearities are irrelevant (attractive interactions), the second method is inefficient.

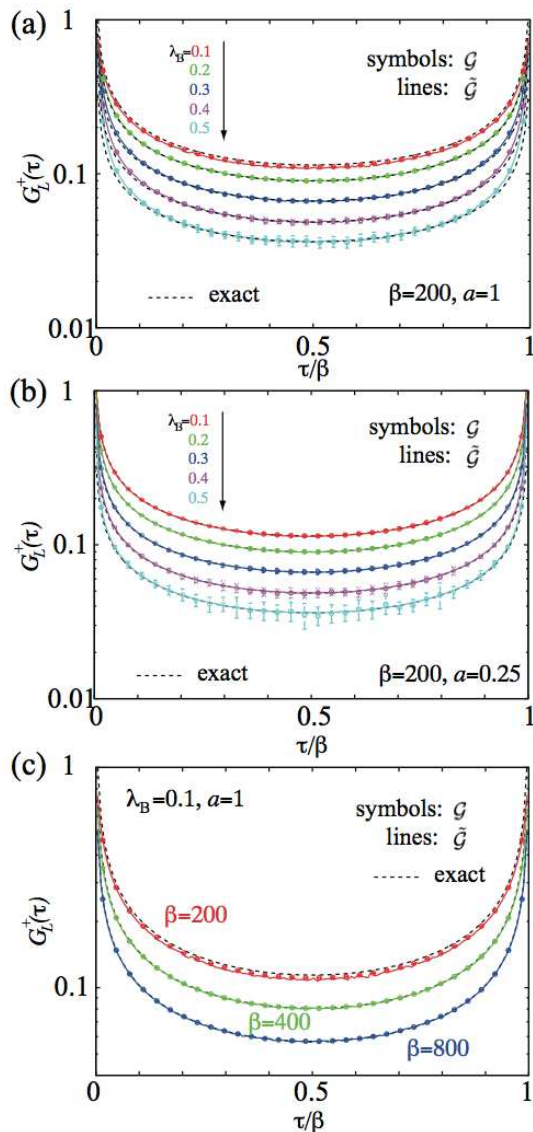


FIG. 1. (Color online) $G_L^+(\tau)$ vs τ/β for several coupling constants $\lambda_B = 0.1$ (top)- 0.5 (bottom) and inverse temperatures β . The exact result (dashed line) is compared to two numerical methods [points with error bars: Eq. (43), solid lines: Eq. (45)]. A comparison of panel (a) (cutoff $a = 1$) to panel (b) (cutoff $a = 0.25$) shows that small deviations from the exact result vanish for small a . Panel (c) shows that highly accurate results can be obtained even for very low T .

3. Universal scaling function for electron Green's function

The main prediction of Kane and Fisher [3] is that for repulsive interactions, $g < 1$, even a weak impurity effectively cuts the chain: Electrons scatter so efficiently from the slowly decaying Friedel oscillations that for $T \rightarrow 0$ and at the Fermi energy one obtains perfect reflection. The fact that the impurity cuts the quantum wire can also be measured by tunneling spectroscopy, i.e., by considering the local Green's function close to the impurity.

Based on the assumption that the wire is perfectly cut by the impurity, one expects for $T = 0$,

$$G_L^+(\tau \rightarrow \infty) \sim \tau^{-1/(2g)}, \quad (48)$$

as has been derived by Furusaki [5]. This prediction can be checked analytically for $g = 1/2$, where an exact analytic result can be derived [4]. Equation (48) should be compared to $G_L^+(\tau \rightarrow \infty) \sim \tau^{-g/2}$ obtained for $\lambda_B = 0$, in the absence of the impurity.

Note that for the computation of the physical electron Green's function one has to consider a further contribution, $G_{LR}(\tau) = -\langle T_\tau \psi_L(\tau) \psi_R^\dagger(0) \rangle$, in addition to $G_L(\tau)$. It is possible to calculate $G_{LR}(\tau)$ using our approach, but we do not discuss it here for simplicity.

From general scaling arguments and the analysis of Kane and Fisher [3], one expects for a weak potential scatterer (small λ_B) a crossover from $G_L^+(\tau \rightarrow \infty) \sim \tau^{-g/2}$ to $G_L^+(\tau \rightarrow \infty) \sim \tau^{-1/(2g)}$ described by a universal (but g -dependent) scaling function \mathcal{F}_g ,

$$G_L^+(\tau) \approx [s(\tau)]^{-g/2} \mathcal{F}_g(T^* \tau, T/T^*), \quad (49)$$

where $[s(\tau)]^{-g/2}$ is the Green's function for $\lambda_B = 0$, see Eq. (??). All dependence on the strength λ_B of the impurity potential is thereby encoded in the characteristic energy scale T^* with

$$T^* = \frac{v}{a} \left(\frac{\lambda_B}{v} \right)^{1/(1-g)}, \quad (50)$$

for small λ_B . The universal scaling form (49) is expected to be valid whenever T^* is much smaller than the cut-off energy v/a . For $T = 0$ and weak λ_B , the short time dynamics is determined by the noninteracting result, $\mathcal{F}_g(x \rightarrow 0, 0) = 1$, while $\mathcal{F}_g(x \rightarrow \infty, 0) \propto x^{(g-1/g)/2}$, see Eq. (48).

In the following, we show our CTQMC results, which confirm the expected behavior and allow us to calculate the full scaling function describing the crossover from weak to strong coupling. To our knowledge, this is the first demonstration of the numerically-exact Green's function in this model.

Figure 2 shows $G_L^+(\tau)/[s(\tau)]^{-g/2}$ versus $T^* \tau$ for several parameter sets (β, λ_B) and (a) $g = 0.3$, (b) $g = 0.5$, and (c) $g = 0.75$ for various temperatures T . Our numerical results reproduce the analytically expected behaviors: First, for wide ranges of λ_B the curves scale on top of each other (we have not used an appropriately rescaled temperature, therefore the upturns occur at different points). Second, we obtain the analytically expected asymptotic behavior with $\mathcal{F}_g(x \rightarrow 0, 0) = 1$, while $\mathcal{F}_g(x \rightarrow \infty, 0) \propto x^{(g-1/g)/2}$, see Eq. (48). Third, our result provides the full crossover function from weak to strong coupling.

To prove that scaling works also at finite T , we show in Fig. 3 $G_L^+(\tau)/[s(\tau)]^{-g/2}$ as a function of τ/β for a wide range of coupling constants λ_B using a fixed ratio of $T/T^* \approx 0.014$. The perfect collapse of the data shows

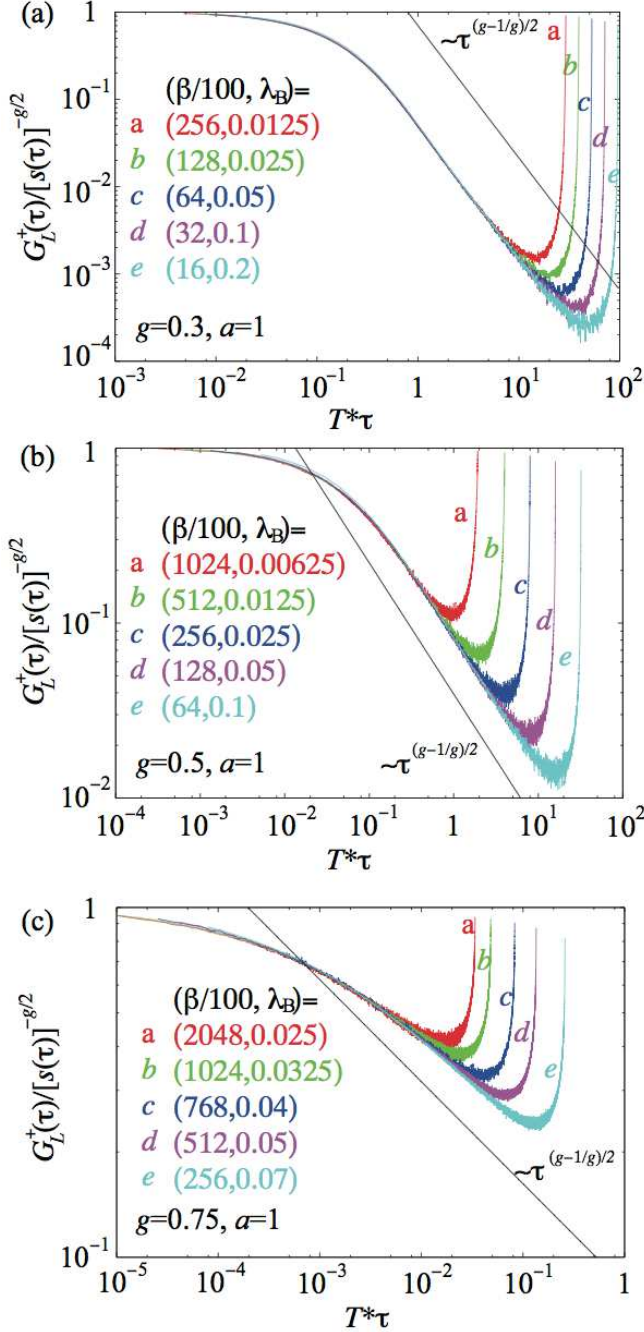


FIG. 2. (Color online) $G_L^+(\tau)/[s(\tau)]^{-g/2}$ versus $T^*\tau$ for various parameter sets (β, λ_B) , $a = 1$ and (a) $g = 0.3$, (b) $g = 0.5$, and (c) $g = 0.75$. Straight lines show the $\tau^{(g-1/g)/2}$ dependence expected from the fixed point where the impurity cuts the chain (the factor $\tau^{g/2}$ originates from the asymptotic form of $[s(\tau)]^{-g/2}$).

that temperature only enters in the combination T/T^* as predicted by Eq. (49).

Finally, we show the $T = 0$ scaling functions $\mathcal{F}_g(x, 0)$ for $g = 0.75$, $g = 0.5$, and $g = 0.3$ in Fig. 4. The $T = 0$ curves can simply be obtained from the small τ data (we use $\tau/\beta < 1/6$) shown in Fig. 2, which are indepen-

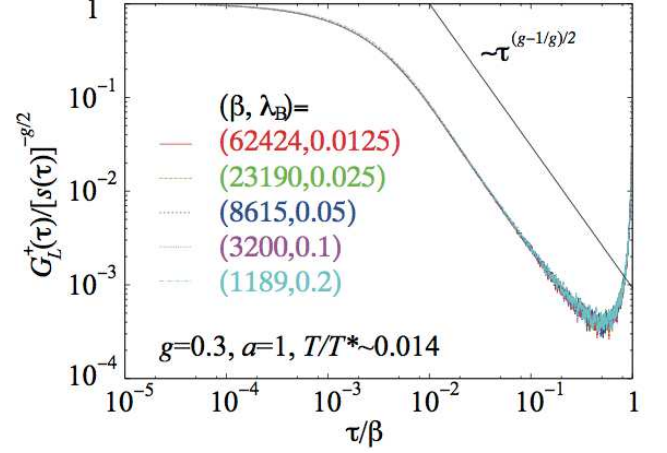


FIG. 3. (Color online) $G_L^+(\tau)/[s(\tau)]^{-g/2}$ vs τ/β for $a = 1$ and various parameters (β, λ_B) keeping the ratio $T/T^* \simeq 0.014$ fixed.

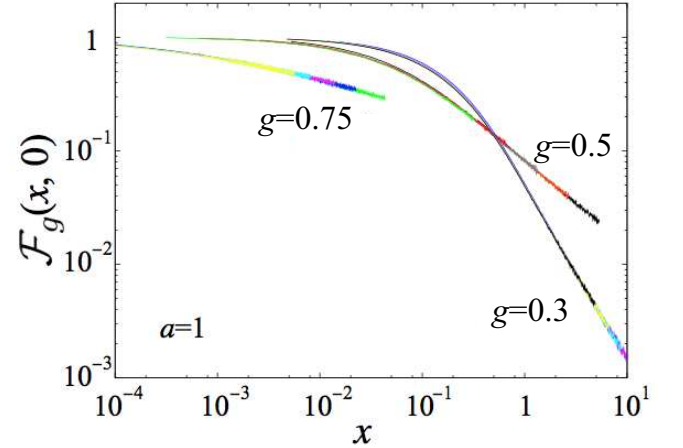


FIG. 4. (Color online) $\mathcal{F}_g(x, 0)$ vs x for $g = 0.75$, $g = 0.5$, and $g = 0.3$ with $a = 1$. Data for $\tau/\beta < 1/6$ of each of the lines in Fig. 2 are used in order to extract the $T = 0$ limit.

dent of β within the scatter of the curve. For g close to 1, T^* becomes exponentially small and it becomes more difficult to extract the low T and long τ results.

B. XXZ Kondo model in helical liquids

Along edges of two-dimensional topological insulators, a special one-dimensional electron system is realized [19]. Namely right- and left-moving electrons have *opposite* spin polarizations, up and down, respectively. The topological protection of these edge channels is reflected by unusual scattering properties: due to time-reversal symmetry a static potential cannot scatter a right-moving spin-up electron into a left-moving spin-down electron.

The situation differs in the presence of a magnetic impurity. Using a spin-flip process, a right mover can be converted in a left mover (and vice versa) due to the

exchange interaction with the quantum impurity. Therefore, it is an interesting problem to study magnetic quantum impurities at the edge of a topological insulator to investigate whether and how topological protection is affected by their presence.

In this subsection, we examine the spin-1/2 XXZ Kondo model [19–21]. We restrict our analysis to the case where the total spin in the z direction is conserved. Although this symmetry is broken in real materials, e.g., by Rashba interactions [23, 24], it is important to clarify also the basic properties of this simplified problem. Note that the transport properties in the presence and absence of this symmetry qualitatively differ as the current in a helical edge state (proportional to $N_\uparrow - N_\downarrow$) can only degrade by processes where spin conservation is violated.

We will use different units from those in the previous subsection, and use the energy unit $v/\xi = 1$ for all g and $\xi = 1$ as a unit of length, in order to use the same high-energy cutoff as in previous studies [19–21]. The main results in this subsection are the phase diagram in g - λ_B plane, which has been discussed perturbatively [19, 21] and the numerically-exact time and temperature dependence of the spin-spin correlation functions for general interaction parameters.

1. Model

For XXZ Kondo model, \hat{X}_F^σ and \hat{X}_B in Eqs. (11) and (12) are given as

$$\hat{X}_F^\pm = \hat{S}^z, \quad \hat{X}_F^- = 1, \quad \text{and} \quad \hat{X}_B = \hat{S}^-. \quad (51)$$

We have used a slightly different quantization axis of the impurity spin from in Refs. [20, 21]: $\hat{S}_z \leftrightarrow -\hat{S}_z$ and $\hat{S}^\pm \leftrightarrow \hat{S}^\mp$. Since V_F^- term is a pure potential scattering in the charge sector and equivalently Φ_- sector, this does not affect the CTQMC and the following discussions, we will concentrate on the Φ_+ sector, $V_F^+ + V_B$, hereafter.

First, we write the Hamiltonian in the bosonization basis

$$\begin{aligned} H = H_{1D} &+ \lambda_F \sqrt{2/g} \partial_x \Phi_+(0) \hat{S}^z + \tilde{\lambda}_B F_L^\dagger F_R \hat{V}_{+\sqrt{2g}}(\Phi_+) \hat{S}^- \\ &+ \tilde{\lambda}_B^* F_R^\dagger F_L \hat{V}_{-\sqrt{2g}}(\Phi_+) \hat{S}^+, \end{aligned} \quad (52)$$

where $\lambda_F = J_z a/2\pi$ describes the coupling of the z -component of the spin, while $\lambda_B = J_\perp a/2\pi$ parametrizes the strength of spin-flip terms [20].

For the CTQMC, it is useful to transform H via a unitary transformation \hat{U} [21],

$$\hat{U} \equiv \exp \left[i \frac{\sqrt{2g}\lambda_F}{gv} \Phi_+(0) \hat{S}^z \right]. \quad (53)$$

This erases the λ_F term in Eq. (52), since

$$\hat{U} H_{1D} \hat{U}^\dagger = H_{1D} - \frac{\sqrt{2g}\lambda_F}{gv} \cdot v \hat{S}^z \partial_x \Phi_+(0). \quad (54)$$

Thus, the Hamiltonian is transformed to

$$\begin{aligned} \hat{U} H \hat{U}^\dagger = H_{1D} &+ \lambda'_B F_L^\dagger F_R \hat{V}_{+\lambda'}(\Phi_+) \hat{S}^- \\ &+ \lambda_B^* F_R^\dagger F_L \hat{V}_{-\lambda'}(\Phi_+) \hat{S}^+, \end{aligned} \quad (55)$$

with $\lambda' = g'\sqrt{2/g}$ and $\lambda'_B = \lambda_B a^{g'/g-1}$, where g' is defined as

$$g' = g - \lambda_F/v. \quad (56)$$

As will be discussed in Appendix B, it is sufficient to consider cases for $\lambda_F \leq gv$, i.e., $\lambda' \geq 0$.

The CTQMC algorithm for this model is similar to that for the Kane-Fisher model. Indeed, an exact relation between the partition functions of the two models is known [25]. Only even $N = 2k$ order terms remain finite due to the fact that the impurity spin is 1/2, i.e., $\hat{S}^+ \hat{S}^+ = \hat{S}^- \hat{S}^- = 0$ and/or the total fermion number conservation. This also restricts configuration space for the impurity spin in Z . We just need to generate configurations in which S^+ and S^- appear alternatively: $\hat{S}^\pm(\tau_1) \hat{S}^\mp(\tau_2) \hat{S}^\pm(\tau_3) \dots$. Thus, we can use algorithm similar to the ‘‘segment’’ representation used in the Anderson model, which accelerates the acceptance rate in the MC samplings [13].

2. Spin-spin correlation function

In this subsection, we explain how to calculate the dynamical spin-spin correlation functions.

First, let us discuss the transverse local spin susceptibility, $\chi^\perp(\tau_{ij}) \equiv [\chi^{+-}(\tau_{ij}) + \chi^{-+}(\tau_{ij})]/2$, where $\chi^{\pm\mp}(\tau_{ij})$ is defined as

$$\chi^{+-}(\tau_{ij}) \equiv \langle T_\tau \hat{S}^+(\tau_i) \hat{S}^-(\tau_j) \rangle. \quad (57)$$

Noting that $\hat{U} \hat{S}^\pm \hat{U}^\dagger = e^{\pm i\sqrt{2g}\lambda_F/(gv)\Phi_+(0)} \hat{S}^\pm$, we can calculate

$$\chi^{+-}(\tau) = \frac{1}{\beta} \left\langle \sum_{ij}^k \mathcal{M}_{ij} \left[\delta(\tau - \tau_{ij}) + \delta(\beta + \tau_{ij} - \tau) \right] \right\rangle, \quad (58)$$

by sampling the following quantity:

$$\begin{aligned} \mathcal{M}_{ij} &= \frac{a^{2g(\frac{\lambda_F}{gv})^2}}{|\lambda'_B|^2} [s(\tau_{ij})]^{-\frac{2\lambda_F}{v}} \left| \frac{\det \hat{S}_{k-1} \{ \tau \ominus \tau_i^-, \tau_j^+ \}}{\det \hat{S}_k \{ \tau \}} \right|^{2g'} \\ &= \frac{a^{2g(\frac{\lambda_F}{gv})^2}}{|\lambda'_B|^2} [s(\tau_{ij})]^{-\frac{2\lambda_F}{v}} \left| (\hat{S}^{-1} \{ \tau \})_{ji} \right|^{2g'}, \end{aligned} \quad (59)$$

where τ_i and τ_j are chosen in a given snapshot $\{\tau\}$ at the $2k$ th order as in Eq. (45) and the corresponding vertex operators at τ_i and τ_j should have $\lambda_i = -\lambda' < 0$ and $\lambda_j = \lambda' > 0$, respectively. For $\chi^{-+}(\tau_{ij})$, the same expression holds with regarding now $\lambda_i > 0$ and $\lambda_j < 0$. We also use symmetry properties $\chi^{\pm\mp}(-|\tau|) = \chi^{\pm\mp}(\beta - |\tau|)$ to obtain results for $0 \leq \tau \leq \beta$. \mathcal{M}_{ij} is, indeed, derived in an almost identical way as in Appendix A 2.

Second, as $U\hat{S}^zU^\dagger = \hat{S}^z$, the longitudinal spin susceptibility is directly evaluated as

$$\chi^z(\tau_{ij}) = \frac{1}{N_{\text{MC}}} \sum_{i=1}^{N_{\text{MC}}} \frac{\langle \hat{S}^\pm(\tau_1) \cdots \hat{S}^z(\tau_i) \cdots \hat{S}^z(\tau_j) \cdots \hat{S}^\mp(\tau_{2k}) \rangle_{\text{imp}}}{\langle \hat{S}^\pm(\tau_1) \cdots \hat{S}^\mp(\tau_{2k}) \rangle_{\text{imp}}}. \quad (60)$$

This is possible because the operator \hat{S}_z does not alter any quantum numbers along the imaginary time axis in CTQMC. In contrast, the transverse susceptibility can be calculated only through the more complicated Eq. (59) [if one would replace $\hat{S}^z(\tau_{i,j})$ by $\hat{S}^\pm(\tau_{i,j})$ in Eq. (60), one would get just zero, since the inserted $\hat{S}^\pm(\tau_{i,j})$ are always next to $\hat{S}^\pm(\tau_\alpha)$ with $\tau_\alpha \in \{\tau\}$].

3. $SU(2)$ check for $g = 1$ and $\lambda_F = \lambda_B$

Interactions at the edge of the quantum wire destroy even for $\lambda_F = \lambda_B$ the $SU(2)$ spin symmetry. In the noninteracting electron limit ($g = 1$), however, the algorithm has to recover $SU(2)$ symmetry for $\lambda_F = \lambda_B$. As the algorithm treats spin-flip and nonflip terms very differently, it is a nontrivial check of the numerical data to see whether $2\chi^z(\tau) = \chi^\perp(\tau)$.

Figure 5 shows $\chi^{z,\perp}(\tau)$ versus τ/β for $\lambda_F = \lambda_B = 0.2$ and $a = 1$. As one can see, the relation $2\chi^z(\tau) = \chi^\perp(\tau)$ holds well. The intrinsic $SU(2)$ symmetry breaking in the Abelian bosonization in our scheme leads to a small $\sim 10\%$ deviations from unity for $\chi^\perp(\tau)/[2\chi^z(\tau)]$ for $a = 1$. These errors do not alter the asymptotic behaviors for $\tau \gg 1$ and we have checked that the expected results $\chi^{z,\perp}(\tau) \sim \tau^{-2}$ for $g = 1$ are reproduced (see also Figs. 8 and 9).

4. Phase diagram

Before starting detailed analysis, we show in Fig. 6 the global phase diagram in the plane spanned by λ_F and g for fixed $\lambda_B = 0.1$. As pointed out in the previous studies [21], there are two phases: the screened phase (SC) where the Kondo effect leads to a screening of the impurity and the local moment (LM) phase where spin-flips are completely suppressed for $T \rightarrow 0$. The phase boundary for $\lambda_B = 0.1$ is well described by the recent renormalization group results for $\lambda_B \ll \lambda_F$ represented by the dashed line [21]. As discussed by Maciejko [21] and also as discussed in Appendix B, the system is symmetric at the solvable “decoupled points” at $\lambda_F = gv$ and the system for $\lambda_F > gv$ can be mapped to that for $2gv - \lambda_B < gv$, and vice versa. Thus, we have only examined the lower part of the boundary in Fig. 6.

The two phases are easily distinguished by the temperature dependence of $\chi^z(\tau)$. For example, Fig. 7 shows the typical behavior of the two phases for $g = 0.3$. For

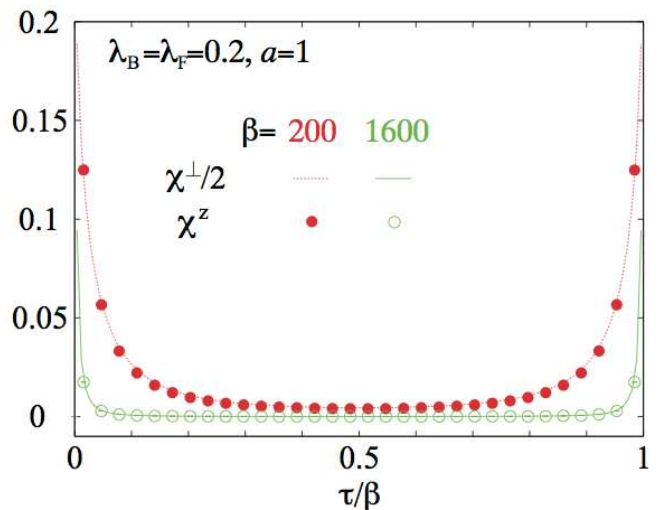


FIG. 5. (Color online) Comparison between $\chi^\perp(\tau)/2$ and $\chi^z(\tau)$ as a function of τ for $\lambda_F = \lambda_B = 0.2$, $a = 1$, and $\beta = 200$ and 1600 .

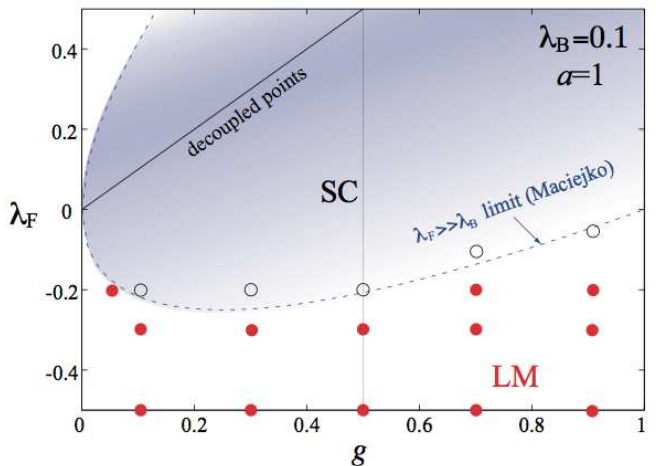


FIG. 6. (Color online) Phase diagram as a function of the TL parameter g and the size of the coupling of the z component of the exchange coupling λ_F for a fixed spin-flip rate $\lambda_B = 0.1$ and $a = 1$. Open (filled) circles indicate the screened (local-moment) phase. For the SC phase, points inside the phase are not indicated and the SC phase is symmetric with respect to the variation of λ_F around the decoupled-point line (see Appendix B). The dashed line represents the phase boundary determined by the renormalization group analysis for $\lambda_F \gg \lambda_B$ [21].

the LM phase ($\lambda_F = -0.5$), $\chi^z(\tau)$ is large and almost τ -independent. Also the T variations are not noticeable on the scale of the plot: the impurity spin is almost free and the spin-flips are strongly suppressed. In contrast, in the SC phase, $\lambda_F = -0.2$, $\chi^z(\tau)$ shows a strong temperature and τ dependence, which reflects screening processes due to the conduction electrons. In the next subsection, we will discuss the low-temperature behaviors of the spin-spin correlation functions in the SC phase.

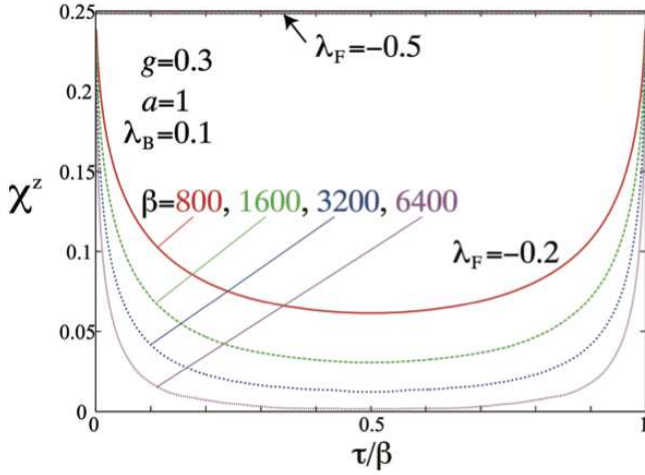


FIG. 7. (Color online) Longitudinal dynamical local spin susceptibility $\chi^z(\tau)$ vs τ/β for $\lambda_F < 0$ and $\lambda_B = 0.1$, $a = 1$, and $\beta = 800$ -6400.

5. Dynamical local spin susceptibility

Figures 8 and 9 show the τ dependence of the spin-spin correlation functions $\chi^\perp(\tau)$ and $\chi^z(\tau)$, respectively, for $\lambda_{B,F} = 0.2$, $\beta = 3200$, and $g = 0.3, 0.5, 0.7$, and 1. We find that the long-time asymptotic decay in the SC phase is given by

$$\chi^\perp(\tau) \sim \tau^{-2g}, \quad (61)$$

while

$$\chi^z(\tau) \sim \tau^{-2} \quad \text{for } g \neq \lambda_F/v. \quad (62)$$

These τ dependencies are also found for $\lambda_F < 0$ as long as one remains in the SC phase as shown in Fig. 10, where $\chi^\perp(\tau)$ are shown for simplicity. The characteristic energy scale becomes smaller and smaller as approaching the phase boundary (increasing g). For $g = 0.5$, $\beta = 6400$ is still not sufficiently low to realize complete τ^{-2g} dependence, while for smaller g 's τ^{-2g} dependence is realized already at $\beta = 3200$.

Near the decoupled point at $\lambda_F = gv$, the leading power-law decay τ^{-2} in $\chi^z(\tau)$ is suppressed and an exponential decay appears, while for $\chi^\perp(\tau)$, there is no such contribution near the decoupled point. These results are consistent with the perturbative analysis in Appendix C. In the following, we will concentrate on the cases for $\lambda_F \neq gv$. Note that the exponent of $\chi^\perp(\tau)$ is precisely given by that at the decoupled point, which is related to the scaling trajectory [21].

These asymptotic forms readily indicate that the local spin susceptibility $\chi^{z,\perp}(T)$ exhibits

$$\chi^{z,\perp}(T) = \int_0^\beta d\tau \chi^{z,\perp}(\tau) \sim T^{2\Delta_{z,\perp}-1} + \text{const.}, \quad (63)$$

where the constant part comes from the short-time cutoff. From our CTQMC results, the scaling dimensions $\Delta_{z,\perp}$

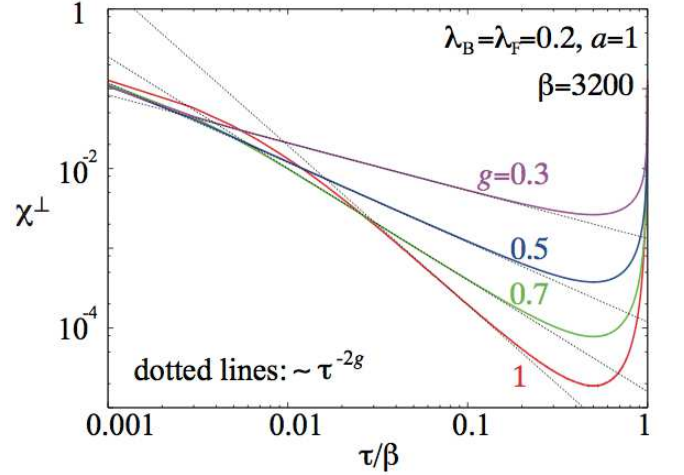


FIG. 8. (Color online) Transverse dynamical local spin susceptibility $\chi^\perp(\tau)$ vs τ for $\lambda_B = \lambda_F = 0.2$, $a = 1$, and $\beta = 3200$. The dotted lines indicate $\sim 1/\tau^{2g}$.

at the screened fixed point are given by

$$\Delta_z = 1 \quad \text{and} \quad \Delta_\perp = g. \quad (64)$$

This is the expected result: Applying a small magnetic field to the screened magnetic impurity is equivalent to applying a local magnetic field to the quantum wire *without* the magnetic impurity. This problem can directly be mapped to the Kane and Fisher problem investigated in the previous subsection. A magnetic field in the z direction induces only forward scattering interaction, which is not renormalized, $\Delta_z = 1$, by the TLL interactions. In contrast, an infinitesimal transverse magnetic field is a relevant perturbation whose scaling dimension g can be read off from Eq. (17).

For $\Delta_\perp = g = 1/2$, there are logarithmic corrections and

$$\chi^\perp(T) \sim -\ln T + \text{const.} \quad \text{for } g = \frac{1}{2}. \quad (65)$$

Thus, the transverse spin susceptibility for $g \leq 1/2$ diverges, while other cases and $\chi_s^z(T)$ stay constant at low temperatures.

These temperature dependencies are indeed obtained from a direct numerical integration of $\chi_s^{z,\perp}(\tau)$. Figure 11 shows $\chi_s^{z,\perp}(T)$ for $\lambda_{B,F} = 0.2$, $a = 1$, $g = 1, 0.7, 0.5$, and 0.3. For $g = 1$, $\chi^\perp(T) = 2\chi^z(T)$ holds due to the SU(2) symmetry. For other values of g 's, $\chi^\perp(T) \neq 2\chi^z(T)$. Figures 11 (b) and 11 (c) show that the susceptibilities follow the predicted power-law of Eq. (63) with high precision for $g = 0.7$ and 0.3 and exhibit the expected logarithmic dependence for $g = 0.5$, see Eq. (65). Note that for $g = 0.7$ we plot $[\chi^\perp(0) - \chi^\perp(T)]/2$ with $\chi^\perp(0)/2 \approx 4.3$ in order to analyze the subleading power-law dependence.

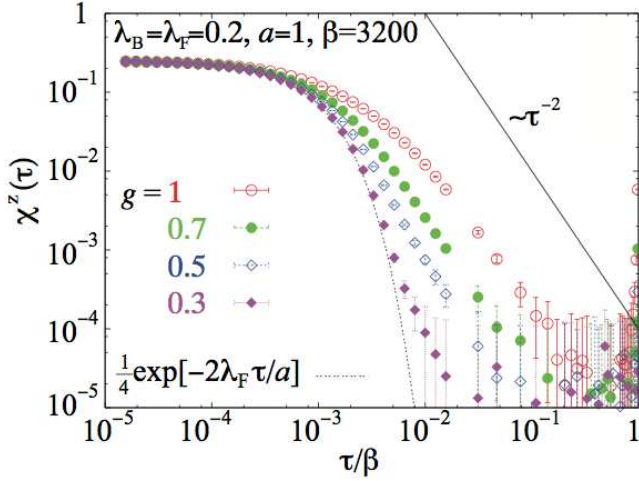


FIG. 9. (Color online) Longitudinal dynamical local spin susceptibility $\chi^z(\tau)$ vs τ for $\lambda_F = \lambda_B = 0.2$, $a = 1$, and $\beta = 3200$. The dashed line shows the exact result for $g = \lambda_F = 0.2$: Eq. (C8), and the line represents $1/\tau^2$.

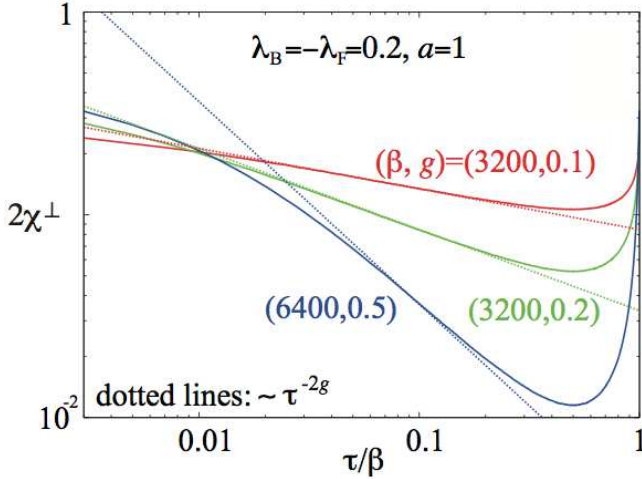


FIG. 10. (Color online) Transverse dynamical local spin susceptibility $\chi^\perp(\tau)$ vs τ for $-\lambda_F = \lambda_B = 0.2$, $a = 1$, and $\beta = 3200$ and 6400 . The dotted lines represent $\sim 1/\tau^{2g}$.

V. DISCUSSIONS

In this section, we will discuss the reliability of some expressions for correlation functions in the “weak-coupling” fixed points and also discuss a possible extension of our method to more complex problems.

A. Correlation functions in the weak-coupling fixed points

For attractive interactions, $g > 1$, in the Kane-Fisher model and for the local moment phase for the XXZ Kondo model, the nonlinear interactions are irrelevant and the system is therefore described by a weak cou-

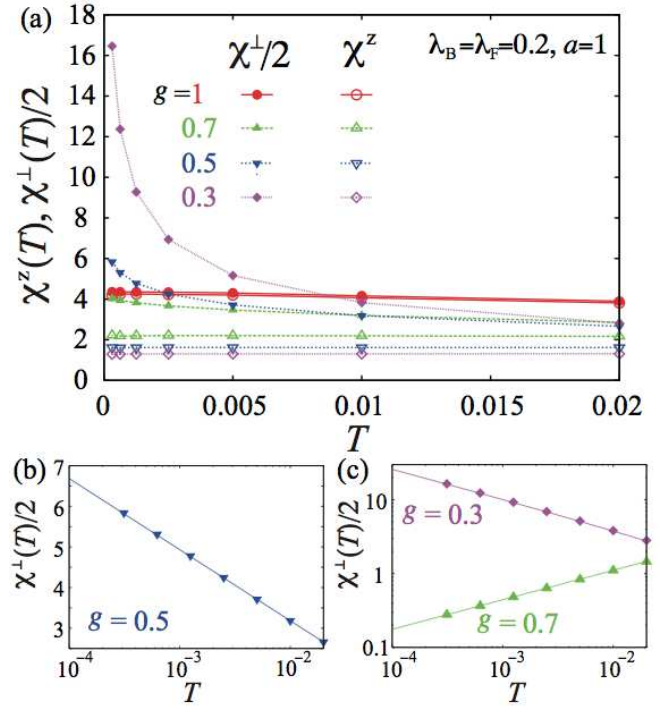


FIG. 11. (Color online) (a) $\chi^z(T)$ and $\chi^\perp(T)/2$ vs T for $\lambda_F = \lambda_B = 0.2$, $a = 1$, and $g = 1, 0.7, 0.5$, and 0.3 . (b) $\chi^\perp(T)/2$ vs T in the log scale for $g = 0.5$. The line indicates the fit by $-0.76 \log(T/0.66)$. (c) $\chi^\perp(T)/2$ vs T for $g = 0.7$ and $g = 0.3$ in the double-log scale. For $g = 0.7$, $4.3 - \chi^\perp(T)/2$ is plotted and the line shows the fit by $7T^{0.4}$. For $g = 0.3$, the line indicates the fit by $-0.396 + 0.66T^{-0.4}$.

pling fixed point. In this regime, not only do the physical properties of the model completely differ (the impurity does not cut the chain and the local moment is not screened) but also the statistical properties of our Monte Carlo sampling change qualitatively. As a consequence, we find that the results based on the method defined by Eqs. (45) and (59) do not give reliable results, while, in contrast, the alternative approach, Eqs. (43) and (60), gives much better results. The reason Eqs. (45) and (59) are not efficient there would be the smallness of overlap between the important configurations for the partition function and those for the Green’s functions. This would be overcome by using a worm algorithm [15]. This is also the reason we use $\chi^z(\tau)$ (not affected by this problem) to identify the two phases in the XXZ Kondo model in Sec. IV B 4.

B. Further applications

Here we discuss briefly further applications of our method for calculating other physical quantities for other models.

For impurity problems, the most important physical quantity is perhaps the conductance. It can naturally be computed within our scheme using that the current

operator at $x = 0$ is expressed by the time derivative of Φ_+ as

$$j(x = 0, \tau) = i \frac{e\sqrt{g}}{2\pi} \partial_\tau \Phi_+(\tau, x = 0), \quad (66)$$

where e is the elementary charge. The correlation function of $j(0, \tau)$ can be effectively calculated in our CTQMC method, and, via analytic continuation to real frequency [22], one can obtain the conductance. This can be done both for the Kane-Fisher and the XXZ Kondo problems. This approach is, however, beyond the scope of our work and will be published elsewhere [26]. Note that an analytic continuation to real frequencies is also needed to calculate, e.g., the tunneling density of states from our results for Green's functions.

Our method can also be directly applied to other scattering problems, involving, for example, the backward scattering of pairs of fermions from nonmagnetic impurities at the edge of a two-dimensional topological insulator [21, 27]. This problem is described by the same Hamiltonian as the Kane-Fisher model but, for example, the tunneling density of states, has to be computed from a different correlator.

In this paper, we have used two-component (L and R) fermionic models as a microscopic model for the bulk TLL. It is straightforward to apply this approach also to spin models or models of bosons in all cases where these models can be described by TLLs. Here one can use standard bosonization identities to map those problems to the ones considered in our paper. It is, however, important to keep track of Klein factors in such mappings. Since our approach fully relies on the noninteracting bosons in the bulk system, it should be emphasized that our method cannot manage interactions of the TLL bosons in the bulk (describing, e.g., Luther-Emery liquids [28] or band-curvature effects).

It would also be highly interesting to study exotic Kondo models coupled to TLLs, which can, e.g., be realized using Majorana modes arising from topological edge states of superconducting islands [29–31] or by using two helical edges [32]. With ultracold atoms, one can also realize Majorana edge mode coupled to a TLL [33]. Knowledge about the dynamics in such problems is not accessible so far, and thus, it is interesting to analyze them on the basis of the CTQMC developed in this paper.

Another technical challenge would be an analysis of impurity problems where two relevant operators compete with each other (arising, e.g., for Kondo models coupled to a helical edge when the spin in z direction is not conserved) and also investigation of multiple and cluster impurities are highly nontrivial. While, for the cases discussed in this paper, no negative-sign problem occurred, this might not be the case for more complex realization

involving several competing scattering channels.

VI. SUMMARY

In summary, we have demonstrated that the continuous-time quantum Monte Carlo method can successfully be applied to situations where a quantum impurity is coupled to an *interacting* one-dimensional quantum wire described by a Tomonaga-Luttinger liquid.

Our method is negative-sign free, which has been proved analytically, and thus, very low temperature calculations are possible as demonstrated. The coding can be realized by a straightforward extension of existing CTQMC codes for purely fermionic problems (without interactions in the environment) as the expression for δZ_{2k} [Eq. (34)] are identical to those of fermionic systems apart from the exponent $2g$. This very simple modification from noninteracting electron system for the bulk part contains all the necessary information about interactions in the bulk system.

We have applied our algorithm to two models. One is the effect of a static scattering potential in a TLL discussed by Kane and Fisher in their classical work [3]. The second is the XXZ Kondo model in the edge of two-dimensional topological insulators [19–21].

For the Kane-Fisher model, we have demonstrated that the long-time asymptotic behavior of electron Green's function is consistent with that predicted by Furusaki [5]. We have also computed the universal scaling function of the Green's function for the first time.

As for the XXZ Kondo model, we have obtained the susceptibilities characterizing the two relevant fixed points: the decoupled local moment fixed point and the screened Kondo fixed point. The temperature dependence and the asymptotic time dependence are consistent with analytic predictions in the whole parameter regime.

The method introduced in this paper is flexible and can be applied to other models and used to study transport properties. We will report analyses of experimentally measurable quantities via analytic continuations and other interesting models in future publications.

ACKNOWLEDGMENT

The authors thank M. Garst and J. Kleinen for fruitful discussions. This work is supported by a Grant-in-Aid for Scientific Research (Grant No. 30456199) from the Japan Society for the Promotion of Science and by the center for Quantum Matter and Materials (QM2) of the University of Cologne. K. H. was supported by Yamada Science Foundation for his long-term stay at the University of Cologne. Some of the numerical calculations were done at the Supercomputer Center at ISSP, University of Tokyo.

[1] S. Tomonaga, Prog. Theor. Phys. **5**, 544 (1950), J. M. Luttinger, J. Math. Phys. **4**, 1154 (1963).

[2] T. Giamarchi, *Quantum Physics in One Dimension*, (Oxford University Press, Oxford, 2004).

- [3] C. L. Kane and M. P. A. Fisher, Phys. Rev. Lett. **68**, 1220 (1992); Phys. Rev. B **46**, 15233 (1992).
- [4] J. v. Delft and H. Schoeller, Ann. Pnys. (Leipzig) **7**, 225 (1998).
- [5] A. Furusaki, Phys. Rev. B **56**, 9352 (1997).
- [6] P. Fendley, H. Saleur, N. P. Wamer, Nucl. Phys. B **430**, 577 (1994), P. Fendley, A. W. W. Ludwig, and H. Saleur, Phys. Rev. Lett. **74**, 3005 (1995), P. Fendley, F. Lesage, and H. Saleur, J. Stat. Phys. **85**, 211 (1996).
- [7] T. Enss, V. Meden, S. Andergassen, X. Barnabé-Thériault, W. Metzner, and K. Schönhammer, Phys. Rev. B **71**, 155401 (2005).
- [8] K. Moon, H. Yi, C. L. Kane, S. M. Girvin, and M. P. A. Fisher, Phys. Rev. Lett. **71**, 4381 (1993).
- [9] K. Leung, R. Egger, and C. H. Mak, Phys. Rev. Lett. **75**, 3344 (1995).
- [10] Y. Hamamoto, K. I. Imura, and T. Kato, Phys. Rev. B **77**, 165402 (2008).
- [11] A. Freyn and S. Florens, Phys. Rev. Lett. **107**, 017201 (2011).
- [12] A. N. Rubtsov, V. V. Savkin, and A. I. Lichtenstein, Phys. Rev. B **72**, 035122 (2005).
- [13] P. Werner, A. Comanac, L. de' Medici, M. Troyer, and A. J. Millis, Phys. Rev. Lett. **97**, 076405 (2006).
- [14] J. Otsuki, H. Kusunose, P. Werner, and Y. Kuramoto, J. Phys. Soc. Jpn **76**, 114707 (2007).
- [15] For review of CTQMC, see, E. Gull, A. I. Lichtenstein, A. N. Rubtsov, M. Troyer, and P. Werner, Rev. Mod. Phys. **83**, 349 (2011).
- [16] A. Georges, G. Kotliar, W. Krauth, and M. J. Rozenberg, Rev. Mod. Phys. **68**, 13 (1996).
- [17] P. Anders, E. Gull, L. Pollet, M. Troyer, and P. Werner, New J. Phys. **13**, 075013 (2011).
- [18] J. Otsuki, Phys. Rev. B **87**, 125102 (2013).
- [19] C. Wu, B. A. Bernevig, and S. C. Zhang, Phys. Rev. Lett. **96**, 106401 (2006).
- [20] J. Maciejko, C. Liu, Y. Oreg, X.-L. Qi, C. Wu, and S.-C. Zhang, Phys. Rev. Lett. **102**, 256803 (2009).
- [21] J. Maciejko, Phys. Rev. B **85**, 245108 (2012).
- [22] M. Jarrell and J. E. Gubernatis: Phys. Rep. **269**, 133 (1996).
- [23] E. Eriksson, A. Ström, G. Sharma, and H. Johannesson, Phys. Rev. B **86**, 161103(R) (2012).
- [24] B. L. Altshuler, I. L. Aleiner, and V. I. Yudson, Phys. Rev. Lett. **111**, 086401 (2013).
- [25] P. Fendley and H. Saleur, Phys. Rev. Lett. **75**, 4492 (1995).
- [26] K. Hattori and A. Rosch, unpublished.
- [27] F. Crépin, J. C. Budich, F. Dolcini, P. Recher, and B. Trauzettel, Phys. Rev. B **86**, 121106(R) (2012).
- [28] A. Luther and V. J. Emery, Phys. Rev. Lett. **33**, 589 (1974).
- [29] B. Béri and N. R. Cooper, Phys. Rev. Lett. **109**, 156803 (2012).
- [30] B. Béri, Phys. Rev. Lett. **110**, 216803 (2013).
- [31] A. Altland and R. Egger, Phys. Rev. Lett. **110**, 196401 (2013).
- [32] T. Posske, C. X. Liu, J. C. Budich, and B. Trauzettel, Phys. Rev. Lett. **110**, 016602 (2013).
- [33] J. Ruhman and E. Altman, arXiv:1401.7343.

Appendix A: Electron Green's function

In this Appendix, we show detailed derivations of Eqs. (43) and (45). A similar analysis is used when we consider the transverse local spin susceptibility in the XXZ Kondo model in Sec. IV B.

1. Equation (43)

First, let us derive Eq. (43). We discuss one configuration in the sampling summation in Eq. (41) with $N_m = 2k$. Setting $\hat{A} = F_L(\tau_i)\hat{V}_{-\eta}(\Phi_+, \tau_i)F_L^\dagger(\tau_j)\hat{V}_\eta(\Phi_+, \tau_j)$ in Eq. (41), we obtain

$$\mathcal{G}_{i>j}^{(2k)} = \frac{\langle T_\tau F_L(\tau_i)\hat{V}_{-\eta}(\tau_i)F_L^\dagger(\tau_j)\hat{V}_\eta(\tau_j)\delta\hat{Z}_{2k}\{\tau\}\rangle_0}{\delta Z_{2k}\{\tau\}}, \quad (\text{A1})$$

with $\tau_i > \tau_j$. Remember that $\eta = \sqrt{g/2}$ and we have abbreviated $\hat{V}_\eta(\Phi_+, \tau)$ simply as $\hat{V}_\eta(\tau)$.

Since the Klein factors and the vertex operators commute, the two sectors are decoupled and the former sector gives $(-1)^{P_{ij}}$ after arranging all the Klein factors in time-ordered product and evaluating the product, where P_{ij} is the number of vertices, or equivalently the number of τ_α , between τ_i and τ_j .

To see this, let us consider a case where P_{ij} is even. It is important to notice that there is no time-dependence in the Klein factors for $l \rightarrow \infty$ [4] and $(F_L^\dagger F_R)(F_R^\dagger F_L) = 1$, since $F_{L,R}^\dagger F_{L,R} = 1$. The Klein factors for $\tau_i > \tau_\alpha > \tau_j$ are rearranged to the form

$$(F_{L,R}^\dagger F_{R,L} F_{L,R}^\dagger F_{L,R} F_{R,L})^{n_p} = (-1)^{n_p} (F_{L,R}^\dagger)^{2n_p} (F_{R,L})^{2n_p}, \quad (\text{A2})$$

with n_p being an integer. Thus, the time-ordered product for $\tau_i \geq \tau \geq \tau_j$ becomes

$$\begin{aligned} & F_L(\tau_i)[(-1)^{n_p}(F_{L,R}^\dagger)^{2n_p}(F_{R,L})^{2n_p}]F_L^\dagger(\tau_j) \\ &= +F_L F_L^\dagger[(-1)^{n_p}(F_{L,R}^\dagger)^{2n_p}(F_{R,L})^{2n_p}]. \end{aligned} \quad (\text{A3})$$

This means the factor arising after the time-ordering is +1 when P_{ij} is even.

When P_{ij} is an odd integer, then the Klein factors for $\tau_i > \tau_\alpha > \tau_j$ are reduced to

$$(-1)^{n_p}(F_{L,R}^\dagger)^{2n_p}(F_{R,L})^{2n_p}F_{L,R}^\dagger F_{R,L}. \quad (\text{A4})$$

Thus,

$$\begin{aligned} & F_L(\tau_i)[(-1)^{n_p}(F_{L,R}^\dagger)^{2n_p}(F_{R,L})^{2n_p}F_{L,R}^\dagger F_{R,L}]F_L^\dagger(\tau_j) \\ &= -F_L F_L^\dagger[(-1)^{n_p}(F_{L,R}^\dagger)^{2n_p}(F_{R,L})^{2n_p}F_{L,R}^\dagger F_{R,L}]. \end{aligned} \quad (\text{A5})$$

These verify that the factor after time-ordering the Klein factors are $(-1)^{P_{ij}} \equiv p_{ij}$.

Now, Eq. (A1) becomes

$$\mathcal{G}_{i>j}^{(2k)} = p_{ij} \frac{\langle \hat{V}_{\lambda_1}(\tau_1) \cdots \hat{V}_{-\eta}(\tau_i) \cdots \hat{V}_\eta(\tau_j) \cdots \hat{V}_{\lambda_{2k}}(\tau_{2k}) \rangle_0}{\langle \hat{V}_{\lambda_1}(\tau_1) \cdots \hat{V}_{\lambda_{2k}}(\tau_{2k}) \rangle_0}. \quad (\text{A6})$$

Here, the product is time-ordered; $\tau_1 > \tau_2 > \dots > \tau_i > \dots > \tau_j > \dots > \tau_{2k}$, and in $\delta Z_{2k}\{\tau\}$ and $\delta \hat{Z}_{2k}\{\tau\}$, we have denoted each vertex operator as $\hat{V}_{\lambda_\alpha}(\tau_\alpha)$ with $\lambda_\alpha = \pm\sqrt{2g}$ ($\alpha = 1, 2, \dots, 2k$). Equation (A6) is calculated by using Eq. (28), leading to

$$\mathcal{G}_{i>j}^{(2k)} = p_{ij} \frac{\prod_{\alpha>\gamma}^{2k\oplus ij} [s(\tau_{\alpha\gamma})]^{\lambda_\alpha\lambda_\gamma}}{\prod_{\alpha'>\gamma'}^{2k} [s(\tau_{\alpha'\gamma'})]^{\lambda_{\alpha'}\lambda_{\gamma'}}}. \quad (\text{A7})$$

Here, in the numerator, if $\alpha, \gamma = i$ or j in the product, $\lambda_i = -\lambda_j = -\eta$. It is evident that factors $s(\tau_{\alpha\gamma})$ within $\{\tau\}$ cancel out and we obtain

$$\begin{aligned} \mathcal{G}_{i>j}^{(2k)} &= p_{ij} [s(\tau_{ij})]^{-\eta^2} \prod_{\gamma}^{2k} [s(\tau_{i\gamma})]^{-\eta\lambda_\gamma} \prod_{\alpha}^{2k} [s(\tau_{\alpha j})]^{\eta\lambda_\alpha} \\ &= p_{ij} [s(\tau_{ij})]^{\frac{g}{2}} \left(\frac{\prod_{\alpha>\gamma}^{2k\oplus ij} [s(\tau_{\alpha\gamma})]^{w_\alpha w_\gamma}}{\prod_{\alpha'>\gamma'}^{2k} [s(\tau_{\alpha'\gamma'})]^{w_{\alpha'} w_{\gamma'}}} \right)^g, \end{aligned} \quad (\text{A8})$$

with $w_{\alpha,\beta} = \text{sgn}(\lambda_{\alpha,\beta})$. Note that the factor g comes from $\eta\lambda_{\alpha,\gamma} = \pm g$. Finally, using the generalized Wick's theorem, we obtain Eq. (43).

2. Equation (45)

Second, we will discuss Eq. (45). This time, the point is that we regard a snapshot $\{\tau\}$ at $2k$ th order as one at $2(k-1)$ th order with the remaining two τ_i and τ_j assigned to each fermion operator for the Green's function.

Suppose that $\tau_i > \tau_j$ and the vertex operator at $\tau_i(\tau_j)$ has $\lambda_i < 0(\lambda_j > 0)$ in a given snapshot $\{\tau\}$, and consider the following quantity:

$$\begin{aligned} \mathcal{Y}_{ij} &\equiv \frac{(-1)^{P_{ij}}}{|\tilde{\lambda}_B|^2} \left([s(\tau_{ij})]^{\lambda_i\lambda_j} \right)^{\frac{1}{4}} \left(\prod_{\gamma \neq i}^{2k} [s(\tau_{i\gamma})]^{\lambda_i\lambda_\gamma} \right)^{-\frac{1}{2}} \\ &\quad \times \left(\prod_{\alpha \neq j}^{2k} [s(\tau_{\alpha j})]^{\lambda_j\lambda_\alpha} \right)^{-\frac{1}{2}}. \end{aligned} \quad (\text{A9})$$

When \mathcal{Y}_{ij} is multiplied to $\delta Z_{2k}\{\tau\}$, we obtain

$$\begin{aligned} \mathcal{Y}_{ij} \delta Z_{2k}\{\tau\} &= \frac{(-1)^{P_{ij}}}{|\tilde{\lambda}_B|^2} [s(\tau_{ij})]^{-\eta^2} \prod_{\gamma \neq i,j}^{2k} [s(\tau_{i\gamma})]^{-\eta\lambda_\gamma} \\ &\quad \times \prod_{\alpha \neq i,j}^{2k} [s(\tau_{\alpha j})]^{-\eta\lambda_\alpha} \delta Z_{2k-2}\{\tau \ominus \tau_i, \tau_j\} \\ &= \langle F_L(\tau_i) \hat{V}_{-\eta}(\tau_i) F_L^\dagger(\tau_j) \hat{V}_\eta(\tau_j) \\ &\quad \times \delta \hat{Z}_{2k-2}\{\tau \ominus \tau_i, \tau_j\} \rangle_0. \end{aligned} \quad (\text{A10})$$

Here, we have used the fact that $\eta = \sqrt{g/2}$ and $\lambda_\alpha = \pm\sqrt{2g}$ with ($\alpha = 1, 2, \dots, 2k$). Then, summing all the configurations $\{\tau\}$ and the perturbation order leads to

$$\sum_{k,\{\tau\}} \mathcal{Y}_{ij} \delta Z_{2k}\{\tau\} =$$

$$\begin{aligned} &\sum_{k,\{\tau\}} \frac{\langle F_L(\tau_i) \hat{V}_{-\eta}(\tau_i) F_L^\dagger(\tau_j) \hat{V}_\eta(\tau_j) \delta \hat{Z}_{2k-2}\{\tau \ominus \tau_i, \tau_j\} \rangle_0}{\delta Z_{2k-2}\{\tau \ominus \tau_i, \tau_j\}} \\ &\times \delta Z_{2k-2}\{\tau \ominus \tau_i, \tau_j\}. \end{aligned} \quad (\text{A11})$$

This indicates that the sampling of \mathcal{Y}_{ij} is indeed equivalent to that of the electron Green's function $G_L^+(\tau_{ij})$. A similar transformation to those used in Eq. (A8) and the generalized Wick's theorem can be applied to Eq. (A9) to obtain Eq. (45), where $\mathcal{Y}_{ij} = \tilde{\mathcal{G}}_{i>j}^{(2k)}$.

Appendix B: Parameter space of the XXZ Kondo model

In this appendix, we briefly discuss that, for the XXZ Kondo model, a system with $\lambda_F^{(1)} > gv$ is equivalent to a model with $\lambda_F^{(2)} = 2gv - \lambda_F^{(1)}$. For example, a very large antiferromagnetic λ_F reduces to a large ferromagnetic $\lambda_F < 0$ in the transformed system. Physically, this happens by binding electrons to the impurity spin. The symmetric point $\lambda_F = gv$ is indeed a solvable point of the present model because $\lambda' = 0$ in Eq. (55). This equivalence is understood as follows. For $\lambda_F > gv$, the Hamiltonian is given as

$$\begin{aligned} UHU^\dagger &= H_{1D} + \lambda'_B F_L^\dagger F_R \hat{V}_{-|\lambda'|}(\Phi_+) \hat{S}^- \\ &\quad + \lambda_B^* F_R^\dagger F_L \hat{V}_{|\lambda'|}(\Phi_+) \hat{S}^+. \end{aligned} \quad (\text{B1})$$

We now interchange the up- and the down-spins for the local moment. Then, since the Klein factors do not matter at all by an appropriate relabeling, the resultant form is equivalent to Eq. (55), if $|\lambda'|$ in Eq. (B1) is equal to λ' in Eq. (55); $\lambda_F^{(1)}/(gv) - 1 = 1 - \lambda_F^{(2)}/(gv)$, with $\lambda_F^{(1)} > gv$ and $\lambda_F^{(2)} < gv$, leading to $\lambda_F^{(1)}/(gv) = 2 - \lambda_F^{(2)}/(gv)$. This symmetry was first taken into account in a recent renormalization group analysis [21].

Appendix C: Spin-spin correlations around decoupled points

In this appendix, we first review the results for decoupled points at $\lambda_F = gv$ in the XXZ Kondo model discussed in Ref. [21]. Then we will discuss the effects of deviations from $\lambda_F = gv$.

a. Decoupled points

In this subsection, we summarize the results of the local spin susceptibilities at decoupled points [21].

For the decoupled points, $\lambda_F = gv$, the Hamiltonian reads

$$\hat{U} H_{\text{dp}} \hat{U}^\dagger = H_{1D} + \frac{\lambda_B}{a} \left[F_L^\dagger F_R \hat{S}^- + \text{H.c.} \right]. \quad (\text{C1})$$

Since the Klein factors do nothing in the following discussions about the spin susceptibilities, this is equivalent to

$$\hat{U}H_{\text{dp}}\hat{U}^\dagger = H_{1D} + h(\hat{S}^+ + \hat{S}^-), \quad (\text{C2})$$

which is just the single-spin Hamiltonian under the magnetic field h parallel to the x direction with $h = \lambda_B/a > 0$ and the bosons and the spin are decoupled. Thus, for any values of λ_B , this can be easily diagonalized.

We now take a new quantization axis parallel to the original x direction, and then

$$\hat{S}^\pm = \tilde{S}^z \mp \frac{1}{2}(\tilde{S}^+ - \tilde{S}^-), \quad \hat{S}^z = \frac{1}{2}(\tilde{S}^+ + \tilde{S}^-). \quad (\text{C3})$$

Let us list correlation functions of \tilde{S} as follows:

$$\tilde{\chi}_{+-}(\tau) = \langle T_\tau \tilde{S}^+(\tau) \tilde{S}^-(0) \rangle = \frac{e^{-2(\beta-\tau)h}}{1 + e^{-2\beta h}}, \quad (\text{C4})$$

$$\tilde{\chi}_{-+}(\tau) = \langle T_\tau \tilde{S}^-(\tau) \tilde{S}^+(0) \rangle = \frac{e^{-2h\tau}}{1 + e^{-2\beta h}}, \quad (\text{C5})$$

$$\tilde{\chi}_{zz}(\tau) = \langle T_\tau \tilde{S}^z(\tau) \tilde{S}^z(0) \rangle = \frac{1}{4}. \quad (\text{C6})$$

The local spin susceptibilities for \hat{S} 's are in linear combinations of Eqs. (C4)-(C6). Thus, we obtain for $T = 0$

$$\chi_{+-}^{\text{dp}}(\tau) = \langle T_\tau \hat{S}^+(\tau) \hat{S}^-(0) \rangle = \frac{1 + e^{-2h\tau}}{4} \left(\frac{a}{v\tau} \right)^{2g}, \quad (\text{C7})$$

$$\chi_{zz}^{\text{dp}}(\tau) = \langle T_\tau \hat{S}^z(\tau) \hat{S}^z(0) \rangle = \frac{1}{4} e^{-2h\tau}. \quad (\text{C8})$$

Here, we have used $\hat{U}\hat{S}^\pm\hat{U}^\dagger = e^{\pm\sqrt{2g}\Phi_+}\hat{S}^\pm$ for $\lambda_F = gv$.

b. perturbations

Let us consider the cases where λ_F slightly deviates from gv : $\delta\lambda_F = \lambda_F - gv$. Then there appears a coupling between the bosons and the local spin as

$$\begin{aligned} \hat{U}\delta H\hat{U}^\dagger &= \delta\lambda_F \sqrt{\frac{2}{g}} \partial_x \Phi_+(0) \hat{S}^z \\ &= \delta\lambda_F \sqrt{\frac{1}{2g}} \partial_x \Phi_+(0) (\tilde{S}^+ + \tilde{S}^-). \end{aligned} \quad (\text{C9})$$

One can calculate the corrections to χ_{zz}^{dp} in the perturbation theory. The second-order perturbation gives

$$\delta\chi_{zz}^{\text{dp}}(\tau) = \frac{[\text{Tr}e^{-\beta H_{\text{dp}}\hat{S}^z(\tau)\hat{S}^z(0)}]^{(2)}}{Z_{\text{dp}}Z_{\Phi_+}^0} - \frac{Z^{(2)}}{Z_{\text{dp}}Z_{\Phi_+}^0} \chi_{zz}^{\text{dp}}(\tau), \quad (\text{C10})$$

where the trace is taken over both the local spin and the Φ_+ boson parts and the superscript (2) indicates the second-order contribution. $Z_{\Phi_+}^0$ is the partition function of free Φ_+ sector and $Z_{\text{dp}} = e^{\beta h} + e^{-\beta h}$. The time dependence that differs from $\chi_{zz}^{\text{dp}}(\tau)$ comes from the first term. At $T = 0$, we find that the power-law dependence appears from

$$\begin{aligned} \frac{[\text{Tr}e^{-\beta H_{\text{dp}}\tilde{S}^-(\tau)\tilde{S}^+(0)}]^{(2)}}{4Z_{\text{dp}}Z_{\Phi_+}^0} &\simeq \frac{\delta\lambda_F^2}{8gZ_{\text{dp}}} \int_0^\tau d\tau_1 \int_0^{\tau_1} d\tau_2 \\ &\times \frac{[\text{Tr}e^{-2\beta h\tilde{S}^z} \tilde{S}^-(\tau)\tilde{S}^+(\tau_1)\tilde{S}^-(\tau_2)\tilde{S}^+(0)]}{v^2(\tau_1 - \tau_2 + a/v)^2} \end{aligned} \quad (\text{C11})$$

$$\equiv \frac{\delta\lambda_F^2}{8gv^2} I_1(2h\tau), \quad (\text{C12})$$

and

$$\begin{aligned} \frac{[\text{Tr}e^{-\beta H_{\text{dp}}\tilde{S}^+(\tau)\tilde{S}^+(0)}]^{(2)}}{4Z_{\text{dp}}Z_{\Phi_+}^0} &= \frac{\delta\lambda_F^2}{8gZ_{\text{dp}}} \int_\tau^{\beta \rightarrow \infty} d\tau_1 \int_0^\tau d\tau_2 \\ &\times \frac{[\text{Tr}e^{-2\beta h\tilde{S}^z} \tilde{S}^-(\tau_1)\tilde{S}^+(\tau)\tilde{S}^-(\tau_2)\tilde{S}^+(0)]}{v^2(\tau_1 - \tau_2 + a/v)^2} \end{aligned} \quad (\text{C13})$$

$$\equiv \frac{\delta\lambda_F^2}{8gv^2} I_2(2h\tau). \quad (\text{C14})$$

Here, in the right-hand side of Eqs. (C11) and (C13), the trace is over the local spin configuration. In the right-hand side of Eq. (C11), we have retained dominant terms for large τ and ignored a diverging term for $T \rightarrow 0$ that cancels out with the second term in Eq. (C10). Note that only terms with $\tilde{S}^+(0)$ are relevant, since a state with $\tilde{S}^z = \downarrow$ is the ground state at the decoupled point. Parameterizing $t = 2h\tau$, $c = 2ha/v$, and $b = 2h\beta \rightarrow \infty$, we obtain

$$I_1(t) = e^{-t} \int_0^t dx \int_0^x dy \frac{e^{x-y}}{(x-y+c)^2} \simeq \frac{1}{t^2} + \dots, \quad (\text{C15})$$

$$I_2(t) = e^t \int_t^b dx \int_0^t dy \frac{e^{-x-y}}{(x-y+c)^2} \simeq \frac{1}{t^2} + \dots. \quad (\text{C16})$$

Thus, finally, we obtain

$$\delta\chi_{zz}^{\text{dp}}(\tau) \simeq \frac{\delta\lambda_F^2}{16g\lambda_B^2} \left(\frac{a}{v\tau} \right)^2. \quad (\text{C17})$$

This indicates that the exponential decay at the decoupled point immediately disappears and the leading term becomes ‘‘Fermi liquid’’ like $\sim \tau^{-2}$.

As for the corrections $\delta\chi_{+-}^{\text{dp}}(\tau)$, there appears at least a factor $\langle \hat{V}_{\sqrt{2g}}(\tau) \hat{V}_{-\sqrt{2g}}(0) \rangle \propto \tau^{-2g}$. Thus, the leading τ dependence of $\chi_{+-}(\tau)$ for $\tau \rightarrow \infty$ does not change from Eq. (C7).